Supporting Information

Structure Design of Hyperbranched Polyamine Adsorbent for CO_2 Adsorption

Hui He[a], Linzhou Zhuang[a], Shuixia Chen[a,b*], Hucheng Liu[a], Qihan Li[a]

a. PCFM Lab, School of Chemistry and Chemical Engineering, Sun Yat-Sen University, Guangzhou 510275, PR China

b. Materials Science Institute, Sun Yat-Sen University, Guangzhou 510275, PR China

Pore structure characterization

Adsorption-desorption isotherms of nitrogen at 77.35 K was measured with an automatic gas adsorption instrument (ASAP2020, Micromeritics Corp, USA) in a relative pressure range from 10^{-6} to 1 after degassing the test sample at 150 °C. Pore volume (V_{total}) was calculated based on the nitrogen amount adsorbed at $P/P_0 = 0.95$. The BET surface areas (S_{BET}) and pore size distribution were calculated through Brunauer-Emmett-Teller (BET) method and density functional theory (DFT) method, respectively.

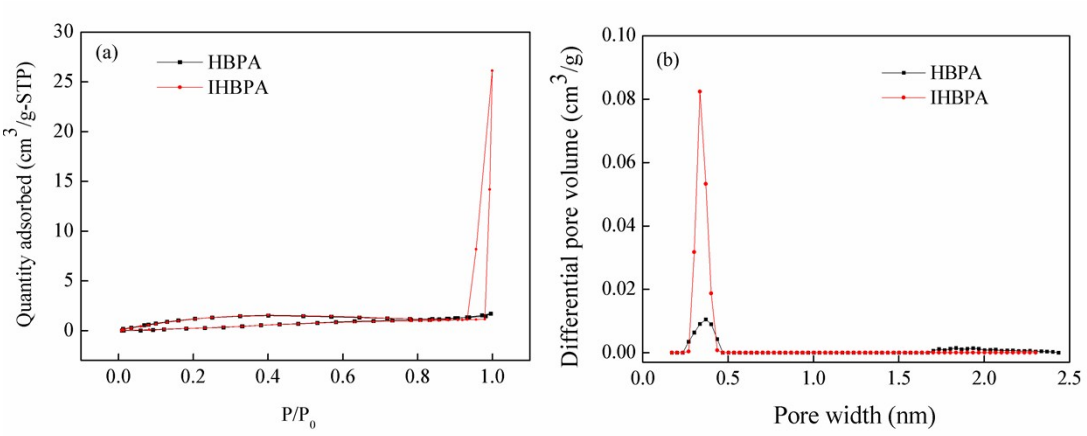

Fig. S1 The N_2 adsorption/desorption isotherms (a) and pore size distributions (b) of

* Corresponding author. *E-mail address*: cescsx@mail.sysu.edu.cn

HBPA(TEPA) and IHBPA(TEPA) by N_2 adsorption-desorption isotherms at 77.35K

From Fig. S1 it is evident that IHBPA(TEPA) had higher porosity at 0.33 nm than HBPA(TEPA). The BET surface area of IHBPA(TEPA) calculated from N_2 adsorption-desorption isotherms at 77.35K have an increment of 12.22 m^2/g from 4.26 m^2/g (HBPA(TEPA)) to 16.48 m^2/g (Table S1). It can be attributed to the micropores formed during the escape of the pre-adsorbed CO_2 from the matrix, demonstrating that the pre-adsorbed CO_2 on HBP-NH_2 would act the role of "imprinting" in the preparation of the adsorbent.

Table S1 The BET surface area and pore volume of HBPA(TEPA) and IHBPA(TEPA)

Materials	BET surface area (m^2/g)	Pore volume (cm^3/g)
HBPA(TEPA)	4.26	0.01
IHBPA(TEPA)	16.48	0.04

Morphology characterization

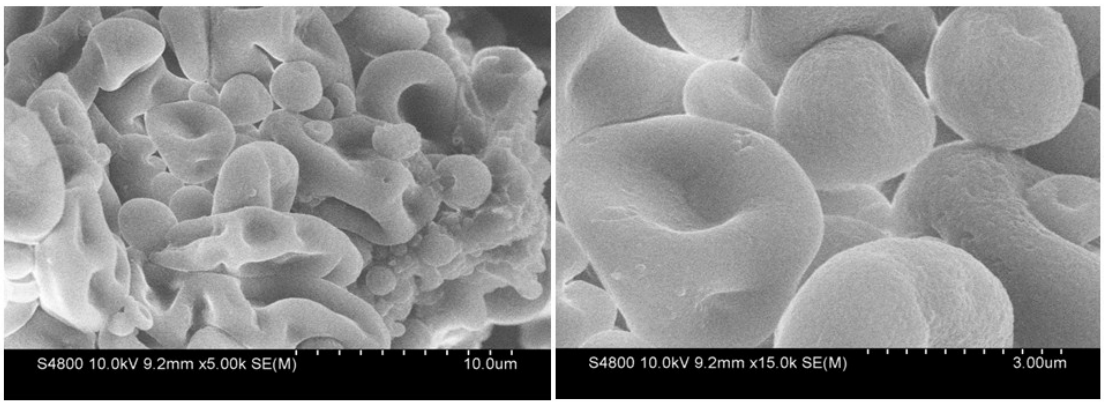

Fig. S2 SEM images of the IHBPA(TEPA)

As shown in Fig. S2, SEM images show the surface morphology of IHBPA(TEPA) particles. It is clear that the IHBPA(TEPA) sample was consist of irregular particles.

CO_2 adsorption kinetics analysis

To better interpret the adsorption behavior and adsorption kinetics of IHBPA-R, the pseudo first-order, pseudo second-order, and Avrami kinetic model were applied to fit the dynamic CO_2 adsorption data at different temperatures.

The equations associated with the kinetic models explored in this work are given as follows.

The pseudo-first order kinetic equation:

$$q_t = q_e[1 - \exp(-k_f t)] \quad \text{(S1)}$$

The pseudo-second order kinetic equation:

$$q_t = \frac{k_s q_e^2 t}{1 + q_e k_s t} \quad \text{(S2)}$$

Avrami:

$$q_t = q_e[1 - \exp(-(k_a t)^{n_a})] \quad \text{(S3)}$$

Where t is the time elapsed from the beginning of the adsorption process, q_t is the amount adsorbed at a given point in time, and q_e represents the amount adsorbed at equilibrium. n is the order of kinetic equation. k_f (1/min), k_s (g/(mmol min)) and k_a (1/min) are rate constants, respectively.

Fig. S3 showed the CO_2 adsorption capacity vs. time at 10 °C, 25 °C, 40 °C, 60 °C, 80 °C, as well as the fitting curves of the three models, while the constants and correlation coefficients based on the stimulation results are presented in Table S2.

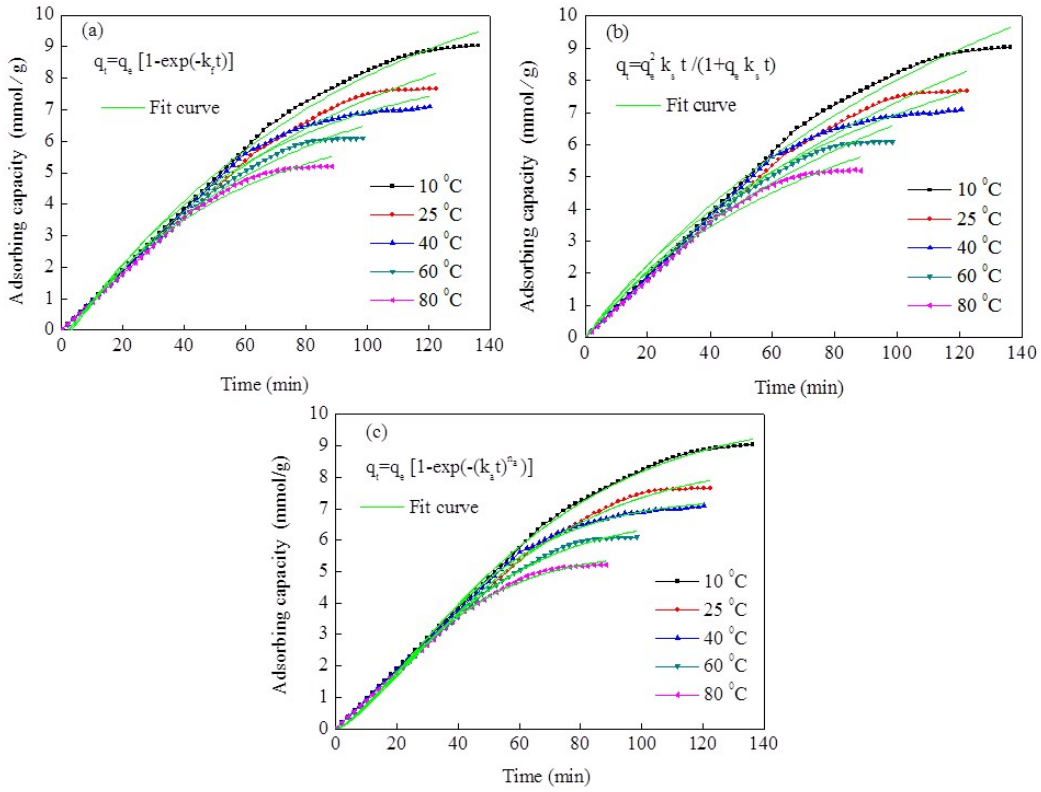

Fig. S3 Plots of pseudo first-order (a), pseudo second-order (b), and avrami (c) kinetic model for CO_2 adsorption on IHBPA(TEPA)-R under different temperature

Fig. S3 (a) and (b) show the pseudo first-order and pseudo second-order plots for CO_2 adsorption on IHBPA(TEPA)-R at different temperatures. It can be found that the experimental data points significantly deviate from the fitting straight curve in the adsorption equilibrium stage, (Fig. S3 (a) and (b)), and the equilibrium adsorption capacity (q_e) also deviate significantly from the experiment value (Table S2). The result indicates that the pseudo first-order and pseudo second-order kinetic model cannot fit the experimental data well, and therefore the physisorption or chemisorption is not the only rate-controlling step. It can be observed that Avrami's kinetic model fit well with the experimental data (Fig. S3 (c)), and the correlation coefficients R^2 for the measured temperatures in Table S2 are in the range of 0.997 to

0.999, while the equilibrium adsorption capacities (q_e) are close to the experiment values, indicating that the Avrami's kinetic model can accurately describe the CO_2 adsorption. The kinetic orders (n_a) are in the range of 1.3 to 1.5, demonstrating that physisorption and chemisorption are both the rate-controlling factors for CO_2 adsorption on IHBPA(TEPA)-R.

Table S2 Kinetic model parameters for CO_2 adsorption on IHBPA(TEPA)-R under different temperature

Kinetic model	Parameter	Temperature (°C)				
		10	25	40	60	80
experimental	q_e(exp)	9.03	7.65	7.09	6.09	5.19
Pseudo-first order model	q_e(fit)	12.36	10.90	8.66	8.57	6.84
	k_f	0.0109	0.0115	0.0166	0.0147	0.0189
	R^2	0.9931	0.9896	0.9930	0.9920	0.9948
Pseudo-second order model	q_e(fit)	22.07	19.93	15.52	14.41	11.84
	k_s	0.00026	0.00029	0.00048	0.00065	0.00086
	R^2	0.9893	0.9820	0.9890	0.9869	0.9909
Avrami	q_e(fit)	9.95	8.53	7.34	6.76	5.60
	k_a	0.0150	0.0165	0.0207	0.02087	0.0253
	n_a	1.3338	1.3630	1.4360	1.3835	1.3654
	R^2	0.9988	0.9979	0.9977	0.9979	0.9980

From the previously shown Table S2, it can be inferred that an increase in

adsorption temperature leads to an increase in k of Avrami kinetic model. This temperature effect also can be demonstrated through the Arrhenius equation (S4), which is the common method to express the adsorption activation energy (E). The following equation is Arrhenius equation:

$$\ln K = -\frac{E}{RT} + \ln A \quad \text{(S4)}$$

where K is the overall mass transfer coefficient, similar to the k_a displayed in Table S2. A is the preexponential factor, E is activation energy (kJ/mol). R is the molar gas constant, and T is the temperature (K).

The activation energy (E) can be analyzed directly from the slope of a plot between lnK and reciprocal of temperature ($1/T$).

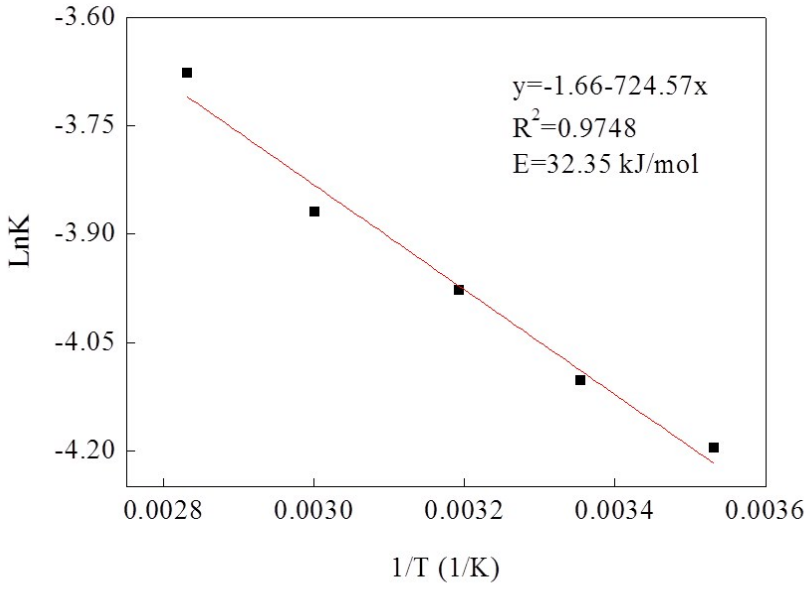

Fig. S4 Arrhenius plots for the kinetic constants obtained by Avrami's kinetic model

The energy for CO_2 adsorption obtained with Arrhenius Eq. (S4) was 32.35 kJ/mol (Fig. S4), which meant that the activation energy for CO_2 desorption from

IHBPA(TEPA)-R was 32.35 kJ/mol. This result was significantly lower than that for CO_2 desorption from PEI-423/MPS [S1] (PEI-423 impregnated into the mesoporous silica, 64.3 kJ/mol), F-PEI423 [S2] (PEI-423 impregnated into the mesoporous foam, 68 kJ/mol), and amine-modified mesoporous silicas (45 to 95 kJ/mol), manifesting that the interaction between the amine of IHBPA(TEPA)-R and CO_2 was relatively weak, which would be advantageous to the regeneration of the adsorbent. One potential explanation was that physisorption, except chemisorption, may play an important role in the CO_2 adsorption of IHBPA(TEPA)-R, and therefore lead to the lower activation energy of CO_2 desorption from IHBPA(TEPA)-R.

Adsorption halftime analysis

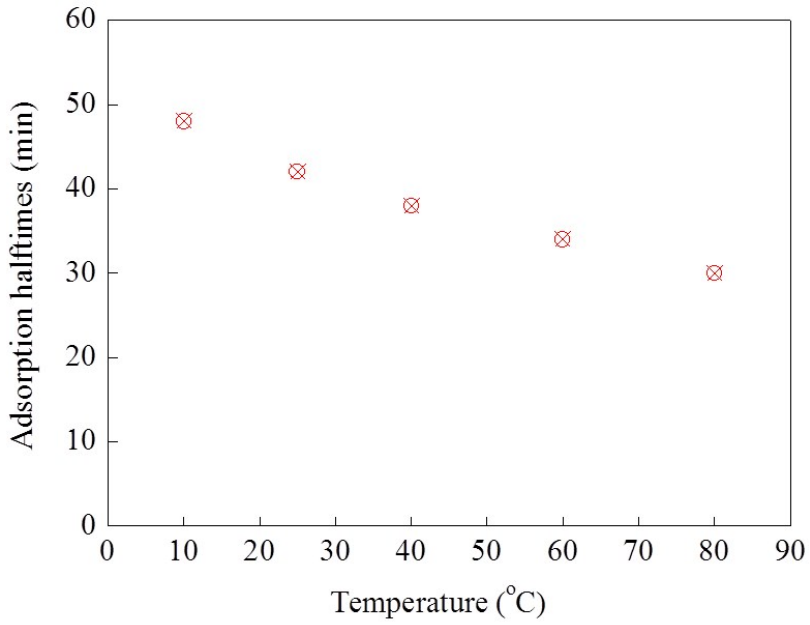

Fig. S5. Adsorption halftimes for CO_2 adsorption on IHBPA-R under different temperature

Given the long times required for some of these adsorbents to approach equilibrium, it is perhaps more reasonable to discuss their kinetics in terms of working capacities that are reported for some time less than the time required to reach full capacity. It is a common practice to use the adsorption halftime (the time where the

adsorbent reaches half of its capacity at the end of the experiment) for this purpose. Fig. S5 shows the adsorption halftimes for the IHBPA-R under different temperatures. At low temperatures, the adsorption halftimes of the IHBPA-R were longer than those at high temperatures, indicating that CO_2 diffusional resistances would be less significant at higher temperatures.

CO_2 adsorption capacity of IHBPA-R in the presence of water

Breakthrough curves were used to characterize the CO_2 adsorption performances of all samples. To test the CO_2 adsorption capacity of IHBPA-R, three conditions were applied. The first condition was that 1.00 g dry adsorbent sample was tightly packed in an adsorption column (Φ= 1.3 cm), into which a dry nitrogen flow was introduced at a flow rate of 30 mL/min for 0.5 h to remove the air in the column. Then, the moist CO_2/N_2 mixed gas (CO_2 : N_2 = 1 : 9 (volume ratio)) was introduced through the column at a flow rate of 30 mL/min (I). The inlet/outlet concentrations of CO_2 were analyzed every two minutes, using a Techcomp 7900 gas chromatograph equipped with a thermal-conductivity detector (TCD). The latter two conditions were that the sample was first immersed in water, then packed in a column (Φ= 1.3 cm), into which a dry nitrogen flow was introduced at a flow rate of 30 mL/min for 0.5 h to remove the air and excess water in the column. Then, the dry (II) or moist (III) CO_2/N_2 mixed gas (CO_2 : N_2 = 1 : 9 (volume ratio)) was introduced through the column at a flow rate of 30 mL/min. After adsorption, pure nitrogen gas at a flow rate of 30 mL/min was introduced through the column at 90ºC to regenerate the spent adsorbent sample. The adsorption capacity was calculated as Equation (1).

$$Q = \int_0^t (C_{in} - C_{eff}) V \mathrm{d}t / 22.4W \qquad (1)$$

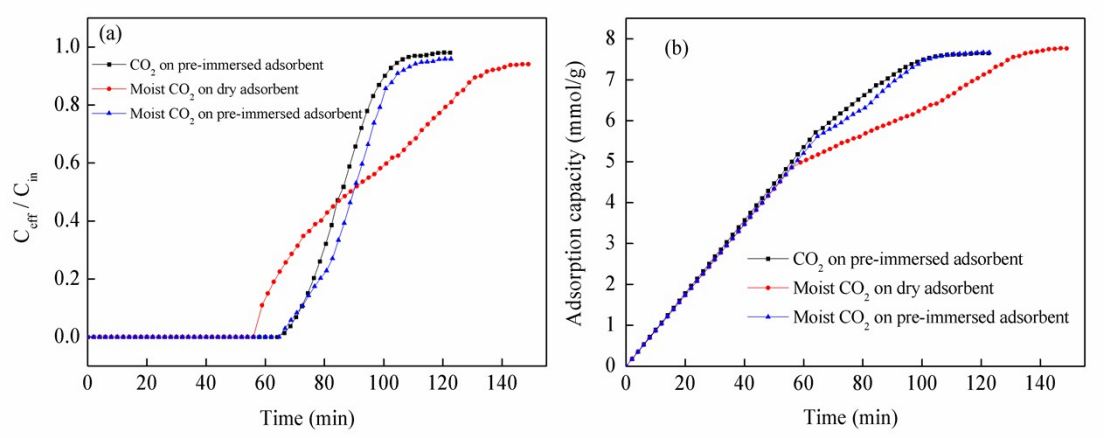

Fig. S6 The adsorption breakthrough curves (a) and adsorption capacity (b) of IHBPA(TEPA)-R under different conditions (adsorbent mass: 1.0 g; adsorption temperature: 25 ^{o}C; concentration of CO_2: 10% (N_2: 27 mL/min; CO_2: 3 mL/min))

The results in Fig. S6 (a) indicated that CO_2 could be completely adsorbed by IHBPA(TEPA)-R adsorbent at the early stage in all three cases, including (I) adsorption of moist CO_2/N_2 mixed gas on dry IHBPA-R adsorbent, (II) adsorption of dry CO_2/N_2 mixed gas on moist IHBPA-R adsorbent, and (III) adsorption of moist CO_2/N_2 mixed gas on moist IHBPA(TEPA)-R adsorbent. The CO_2 adsorption capacities of IHBPA(TEPA)-R in the 3 case all remained at 7.65 ~ 7.77 mmol/g (Fig. S6 (b)), demonstrating that CO_2 adsorption capacity measured by using pre-humidified adsorbent could be applied to characterize its working adsorption capability. The results are comparable.

The comparison of the adsorption breakthrough curves of case I with case II or III (Fig. S6 (a)) also indicate that adsorbent pre-swollen[S3, S4] could fast adsorb CO_2 and took a shorter time to achieve its equilibrium adsorption (case II or III).

REFERENCES

S1. M. J. Al-Marri, M. M. Khader, M. Tawfik, G. Qi, and E. P. Giannelis, *Langmuir*, 2015, 31, 3569-3576.

S2. G.G. Qi, L. L. Fu, B. H. Choi and E. P. Giannelis. *Energ. Environ. Sci.*, 2012, 6,

7368-7375.

S3. Z. H. Chen, S. B. Deng, H. R. Wei, B. Wang, J. Huang and G. Yu, *ACS Appl. Mater. Interfaces*, 2013, 5, 6937-6945.

S4. W. R. Alesi and J. R. Kitchin, *Ind. Eng. Chem. Res.*, 2012, 51, 6907-6915.